**Atmospheric
Measurement
Techniques
Discussions**

Using sonic anemometer temperature to measure sensible heat flux in strong winds

S. P. Burns[1,2], T. W. Horst[1], P. D. Blanken[2], and R. K. Monson[3]

[1]National Center for Atmospheric Research, Boulder, Colorado, USA
[2]Department of Geography, University of Colorado, Boulder, USA
[3]School of Natural Resources and the Environment, University of Arizona, Tucson, USA

Correspondence to: S. P. Burns (sean@ucar.edu)

Title Page

Abstract	Introduction
Conclusions	References
Tables	Figures

◄◄	►►
◄	►
Back	Close

Full Screen / Esc

Printer-friendly Version

Interactive Discussion

S. P. Burns et al.

Title Page

Abstract	Introduction
Conclusions	References
Tables	Figures

|◄ | ►|

◄ | ►

| Back | Close |

Full Screen / Esc

Printer-friendly Version

Interactive Discussion

Abstract

The sensible heat flux (H) is a significant component of the surface energy balance (SEB). Sonic anemometers simultaneously measure the turbulent fluctuations of vertical wind (w') and sonic temperature (T_s'), and are commonly used to measure H. Our study examines 30-min heat fluxes measured with a Campbell Scientific model CSAT3 sonic anemometer above a subalpine forest. We compare H calculated with T_s to H calculated with a co-located thermocouple and find that for horizontal wind speed (U) less than $8\,\mathrm{m\,s^{-1}}$ the agreement is $\approx \pm\,30\,\mathrm{W\,m^{-2}}$. However, for $U >\approx 8\,\mathrm{m\,s^{-1}}$, the CSAT3 H becomes larger than H calculated with the thermocouple, reaching a maximum difference of $\approx 250\,\mathrm{W\,m^{-2}}$ at $U \approx 18\,\mathrm{m\,s^{-1}}$. H calculated with the thermocouple results in a SEB that is relatively independent of U at high wind speeds. In contrast, the SEB calculated with H from the CSAT3 varies considerably with U, particularly at night. Cospectral analysis of $\overline{w'T_s'}$ suggest that spurious correlation is a problem during high winds which leads to a positive (additive) increase in H calculated with the CSAT3. At night, when H is typically negative, this CSAT3 error results in a measured H that falsely approaches zero or even becomes positive. Within a broader context, the usefulness of side-by-side instrument comparisons are discussed.

1 Introduction

Sonic anemometers have been used to measure three-dimensional wind vectors, temperature, and surface sensible heat and momentum fluxes since the early 1960s. They have played a pivotal role in studying the surface energy balance (SEB), which describes how the radiative energy at the earth's surface is partitioned between latent heat flux (evaporation and transpiration of water to the atmosphere) and sensible heat flux (heat exchange between the surface elements, ground, and atmosphere) (Stewart and Thom, 1973; Garratt, 1992; Blanken et al., 1997; Oncley et al., 2007; Foken, 2008). Despite improvements in instrumentation accuracy, most flux-measuring sites

find that the measured sensible and latent heat fluxes only account for ≈80 % of the available incoming energy (Wilson et al., 2002; Foken, 2008). The so-called "energy balance closure problem" has recently been reviewed (Foken, 2008; Foken et al., 2011) and the conclusion was reached that the imbalance can be mostly attributed to low-frequency flux contributions from heterogenous landscapes which are not measured by eddy-covariance techniques. The energy balance closure typically improves under windy/turbulent conditions when the ground and atmosphere are "well-coupled" (Franssen et al., 2010). Spatially homogeneous and moisture-limited environments such as deserts appear to be optimal for successfully closing the energy budget (Timouk et al., 2009; Foken, 2008).

This paper uses data from the Niwot Ridge Subalpine Forest AmeriFlux site (NWT) to examine the sensible heat flux with strong winds. Turnipseed et al. (2002) studied the energy balance at the NWT site and found that during the daytime the sum of the turbulent fluxes accounts for 80–90 % of the radiative energy input into the forest. At night, under moderately turbulent conditions, the energy balance closure is comparable to the daytime. However, when the nighttime conditions are either calm or extremely turbulent, the sensible and latent heat fluxes only account for 20-60 % of the net longwave radiative flux. Turnipseed et al. (2002) discussed several possible reasons for this nighttime discrepancy (e.g., instrument error, footprint mis-match, horizontal advection), but none of these reasons could adequately explain the fact that the nighttime imbalance persisted in the presence of strong winds. They concluded that the sonic temperature did not have sufficient resolution to capture the small temperature fluctuations which led to inaccurate sensible heat fluxes.

In early 2008 the sonic anemometers at NWT were re-calibrated (details in Sect. 2.3). After the recalibration, the new sensible heat flux still did not improve the agreement between the daytime and nocturnal energy balance in windy conditions, and the imbalance was even more dramatic than before the re-calibration. The goals of the current study are to: (1) describe the discrepancy observed in the calculated sensible heat flux, (2) compare the sensible heat flux calculated using sonic temperature to that calculated

with a co-located thermocouple, and (3) re-visit the surface energy balance results from Turnipseed et al. (2002) in light of the results from item (2).

2 Data and methods

2.1 Site description

This study uses data from the Niwot Ridge Subalpine Forest AmeriFlux site (40°1′58″ N, 105°32′47″ W, 3050 m elevation, data version 2011.04.20). The site is located below Niwot Ridge, Colorado, 8 km east of the Continental Divide. The NWT measurements started in November 1998 as described in Monson et al. (2002) and Turnipseed et al. (2002, 2003). The tree density around the NWT Tower is ≈0.4 trees m^{-2} with a leaf area index (LAI) of 3.8–4.2 m^2 m^{-2} and tree heights of 12–13 m (Turnipseed et al., 2002). In winter, NWT is a windy place. Between November–February, the 30-min average 21.5 m wind speed (U) is around 7 m s^{-1} (standard deviation ≈4.5 m s^{-1}) with a maximum U near 20 m s^{-1}. More information on NWT is available on-line at http://public.ornl.gov/ameriflux/.

2.2 Sonic anemometer thermometry

A few of the important relationships related to sonic anemometer thermometry are summarized here; a more complete description of the technology is readily available (e.g., Kaimal and Businger, 1963; Schotanus et al., 1983; Kaimal and Gaynor, 1991; Loescher et al., 2005, and many others).

A sonic anemometer-thermometer calculates air temperature (T) by measuring the speed of sound (c). The relationship between air temperature, the speed of sound, and specific humidity (q) within the atmosphere is well-known,

$$T = \frac{c^2}{\gamma_d\, R_d} \left(\frac{1}{1 + 0.51q} \right),$$
(1)

Printer-friendly Version

Interactive Discussion

where $\gamma_d = c_p/c_v = 1.4$ is the dry air specific heat ratio and R_d is the gas constant for dry air ($287.04 \, \mathrm{J \, kg^{-1} \, K^{-1}}$).

A sonic anemometer-thermometer sequentially transmits and receives sound pulses between two transducers separated by a path-length distance (d). The sonic temperature (T_s) is determined from the measured times to transit d (t_1 in one direction and t_2 in the opposite direction) and the geometry of the sound rays such that,

$$T_s \equiv \frac{c^2}{\gamma_d R_d} = \frac{1}{\gamma_d R_d} \left[\left(\frac{d}{2}\right)^2 \left(\frac{1}{t_1} + \frac{1}{t_2}\right)^2 + V_n^2 \right],$$ (2)

where V_n is the wind component perpendicular to d (i.e., cross-wind). Equation (2) is for dry air.

In a real atmosphere (i.e., one with water vapor), air temperature is calculated from T_s as $T_s^{\mathrm{air}} = T_s (1 + 0.51q)^{-1}$. If the measured variables are decomposed into mean and fluctuating components (e.g., $T = \overline{T} + T'$, etc., see Schotanus et al., 1983), then the sensible heat flux H is calculated with,

$$H = \rho \, c_p \, \overline{w'T'} = \rho \, c_p \left[\overline{w'T_s'} - 0.51 \, \overline{T} \, \overline{w'q'} + 2 \frac{\overline{T} \, \overline{u}}{\overline{c^2}} \, \overline{u'w'} \right],$$ (3)

where ρ is the air density, c_p is the specific heat of air at constant pressure, and u and w are the horizontal and vertical wind components in streamwise coordinates. The $\overline{u'w'}$ term is the so-called cross-wind correction term and most modern sonic anemometers take this into account with internal processing software (Loescher et al., 2005; Campbell Scientific, 2011).

2.3 Energy balance equation and instrumentation

The terms in the surface energy balance are,

$$R_a = R_{\mathrm{net}} - G - S_{\mathrm{canopy}} - S_{\mathrm{soil}} = H + LE,$$ (4)

Sensible heat flux in high winds

S. P. Burns et al.

where R_a is the "available energy". At NWT, net radiation (R_{net}) was measured at $z \approx 25$ m above the ground with both a net (Radiation and Energy Balance Systems – REBS, model Q*7.1) and four-component (Kipp and Zonen, model CNR-1) radiometer. The soil heat flux (G) was measured with multiple soil heat flux plates (REBS, Model

5   HFT-1) at a depth of −10 cm. The two storage terms (S_{canopy} and S_{soil}) account for the heat stored between the ground and the flux measurement heights, and are typically less than 10 % of R_{net} (Oncley et al., 2007). At NWT, Turnipseed et al. (2002) showed that the storage terms and G were small (less than 8 % of R_{net}) and we neglect S_{canopy} and S_{soil} for this study.

10   Latent heat flux (LE), and H were measured at $z \approx 21.5$ m with a Campbell Scientific model CSAT3 sonic anemometer (hereafter "CSAT"; Campbell Scientific, 2011) providing the high-frequency vertical wind (w') and temperature (T_s') fluctuations, while water vapor (q') was measured with a co-located krypton hygrometer (Turnipseed et al., 2002). Winds are rotated from sonic to planar-fit coordinates prior to the flux

15   calculations (Wilczak et al., 2001). T_s output by a CSAT is an average from three non-orthogonal paths. We use "H_{CSAT}" to designate H calculated with T_s following Eq. (3). In our discussions, SEB refers to the ratio of the sum of the turbulent fluxes to ($R_{net} - G$), i.e., SEB $= (H + LE)/(R_{net} - G)$.

The CSAT can operate with either embedded code version 3 or version 4 (hereafter,

20   ver3 and ver4) and uses advanced digital signal processing to determine the ultrasonic times of flight (e.g., t_1 and t_2 in Eq. 2). Ver4 is designed to produce usable results when the signal is weak such as when liquid water is on the transducers, but degrades the T_s resolution from 0.002 °C in ver3 to 0.03 °C in ver4 (see Campbell Scientific, 2011 for more details about ver3 versus ver4).

25   Here, we briefly summarize the sequence of events that led to our study (also see Table 1). In 2008 we sent the three University of Colorado (CU) CSATs (all ver3) back to Campbell Scientific, Inc. for re-calibration and one of them (sn 0328) was upgraded to ver4. After deploying the ver4 CU CSAT at 21.5 m, we observed nighttime H_{CSAT} values that were frequently above zero, indicating heat was being transported from

the surface to the atmosphere at night. Though such conditions are possible for short periods (e.g., due to warm air advection), we have rarely observed such phenomena in the previous 10 years of measurements. These anomalous H_{CSAT} measurements were strongly correlated with high winds (Fig. 1).

Because we were curious/suspicious about these above-zero nighttime H_{CSAT} values, we deployed a CSAT from the National Center for Atmospheric Research (NCAR) Earth Observing Laboratory (EOL) at the same level as the CU CSAT (ver4). The EOL CSAT initially used ver3, which we changed to ver4 partway through our study (Table 1). To change from ver3 to ver4, the processing chip in the CSAT electronics enclosure was changed, but the sonic head was not disturbed. Additional air temperature information was provided near the 21.5 m level by a 0.254 mm E-type thermocouple that was located about 1.4 m from the CU CSAT and sampled at 1-Hz. Because we were concerned about flux loss due to horizontal separation and lack of high-frequency sampling, a second E-type thermocouple was deployed in May 2010 within 5 cm of the CU CSAT transducers and sampled at 10-Hz. The thermocouple temperature fluctuations (T'_{tc}) are correlated with w' from the CU CSAT to calculate a sensible heat flux (e.g., $H_{T_{tc}} = \rho c_p \overline{w'T'_{tc}}$). The other temperature sensor at the 21.5 m level was a mechanically-aspirated slow-response temperature-humidity sensor (Vaisala HMP35-D probe) which we use as a "reference" sensor for time-averaged comparisons.

3 Results and discussion

3.1 Comparison of sensible heat fluxes

If H is calculated using the EOL CSAT, CU CSAT, and T_{tc} there are large H differences during periods of strong winds that are most obvious at night (Fig. 1). In a perfect sonic anemometer the path-length d is constant, however real world changes to d can occur as the sensor material expands and contracts due to temperature changes or wind-induced stresses or vibrations. Lanzinger and Langmack (2005) use a Thies

Back | Close

Full Screen / Esc

Printer-friendly Version

Interactive Discussion

two-dimensional sonic anemometer to show that a 50 K temperature change results in a 0.4 mm change in d which produces a 1.2 K error in T_s. We did not observe any temperature-dependent H differences in our study.

After separating the H data by day and night, there is a consistent trend in the $H_{CSAT} - H_{T_{tc}}$ difference; for $U > \approx 8 \, \mathrm{m \, s^{-1}}$, H_{CSAT} becomes more positive than $H_{T_{tc}}$ and the difference increases as U increases up to a difference of $\approx 250 \, \mathrm{W \, m^{-2}}$ at $U \approx 17 \, \mathrm{m \, s^{-1}}$ (Fig. 2). Our original supposition that this was primarily a nighttime problem is incorrect because the daytime and nighttime differences are qualitatively similar. We have separated the panels of Fig. 2 into periods when different configurations of CSATs were on the tower (Table 1). By comparing Fig. 2a and 2b we find that H_{CSAT} EOL ver3 agreed better with $H_{T_{tc}}$ than H_{CSAT} EOL ver4. Also, $H_{CSAT} - H_{T_{tc}}$ for EOL CSAT ver3 did not have as strong a dependence on U as ver4.

One issue of concern with $H_{T_{tc}}$ (1-Hz) is the $\approx 1.4 \, \mathrm{m}$ horizontal sensor separation between the CU CSAT (w') and 1-Hz thermocouple (T'_{tc}) (Horst and Lenschow, 2009). If one compares $H_{CSAT} - H_{T_{tc}}$ using T_{tc} 1-Hz (Fig. 2c) with T_{tc} 10-Hz (Fig. 2d), the trend of increasing H difference with increasing U is apparent for both thermocouples. This encourages us that H calculated with T_{tc} (1-Hz) results in a viable heat flux; furthermore, as one would expect, $H_{T_{tc}}$ (10-Hz) has reduced scatter in $H_{CSAT} - H_{T_{tc}}$. Though $H_{T_{tc}}$ (1-Hz) and $H_{T_{tc}}$ (10-Hz) appear similar, there are some differences between them which are discussed below. We should note that it would be useful to confirm that T_{tc} (10-Hz) is adequately capturing the high-frequency ($f > \approx 2 \, \mathrm{Hz}$) portion of $\overline{w'T'_{tc}}$. However, a visual comparison with previously published $\overline{w'T'}$ cospectra (e.g., Kaimal and Finnigan, 1994; Blanken et al., 1998; Massman and Clement, 2005) suggest that our results are reasonable.

In order to make a connection to the older heat flux data (e.g., data collected between 1998–2008), we examine CU CSAT ver3 $H_{CSAT} - H_{T_{tc}}$ (1-Hz) from a period prior to the CSAT recalibration (Fig. 2e). The dependence of $H_{CSAT} - H_{T_{tc}}$ on U is similar to that observed with the other CSATs. This result is important in our consideration of the

energy budget (Sect. 3.2) and to make a link to the results from Turnipseed et al. (2002).

To gain further insight into the $H_{\mathrm{CSAT}} - H_{T_{\mathrm{tc}}}$ differences, we examine the spectra of w', T'_{s}, and T'_{tc} and their associated cospectra and ogives (Friehe et al., 1991) for high-wind conditions (Fig. 3). The S_w and S_T spectra from the two CSATs are in good agreement, but show the effect of high-frequency noise and aliasing. S_T from T_{tc} (10-Hz) is attenuated at frequencies above ≈ 1 Hz because the thermal mass of the thermocouple wire limits the response time. In high-wind conditions (e.g., when the S_w and S_T energy peak is shifted to higher frequencies) we observe that $H_{T_{\mathrm{tc}}}$ (1-Hz) is about 10–20 % smaller than $H_{T_{\mathrm{tc}}}$ (10-Hz) due to the lower sampling rate as well as the horizontal separation. During the day the low-frequency part of S_T and $(Co)_{wT}$ for the CSAT and thermocouple are in fairly good agreement (Fig. 3a). At night, however, S_T from T_{tc} has more energy than T_{s}, and $(Co)_{wT_{\mathrm{tc}}}$ differs dramatically from the cospectra of the two CSATs. The H ogive reveals nocturnal $H_{T_{\mathrm{tc}}} \approx -90\,\mathrm{W\,m^{-2}}$ compared to $H_{\mathrm{CSAT}} \approx -30\,\mathrm{W\,m^{-2}}$ (Fig. 3b). It appears there is spurious correlation in $\overline{w'T'_{\mathrm{s}}}$ that enhances $(Co)_{wT_{\mathrm{s}}}$ during the day and degrades it at night. As U becomes smaller, the spectra and cospectra come into better agreement (Fig. 4).

We considered the possibility of tower/sonic vibration or movement affecting the transit times (e.g., t_1 and t_2 in Eq. 2) and causing the $\overline{w'T'_{\mathrm{s}}}$ error. However, the main source of the problem appears to be with T'_{s} not w' because $\overline{w'T'_{\mathrm{tc}}}$, which uses the same CSAT w', produces reasonable heat fluxes, e.g., predominantly negative H at night. Also, similar high-frequency noise in CSAT S_T (not shown here) have been observed on a 30-m tower during high-winds in the CHATS field project (Patton et al., 2011). This suggests the problem is not specific to the NWT tower. Furthermore, discussions with Campbell Scientific, Inc. engineers have also led us to believe that sensor movement is not the cause of the problem. Without an independent measure of w' it is difficult to check the vertical wind, but we note that S_w in high winds is flatter than the expected $-2/3$ slope (Fig. 3a–b). Finally, we also considered the $\overline{w'q'}$ and $\overline{u'w'}$ terms in Eq. (3),

but found them too small to explain the discrepancy between H_{CSAT} and $H_{T_{tc}}$ (results not shown).

In order to look further at the possibility of errors in T_s, we compare T_s^{air} and T_{tc} to an aspirated temperature-humidity sensor (T_{asp}) as a function of U. At night (Fig. 5a and b), the $T_{tc} - T_{asp}$ difference is less than $\pm0.1\,^{\circ}$C and independent of U. However, during the day (Fig. 5c and d) there is a well-known radiation effect on T_{tc} that causes it to be larger than T_{asp} by about $0.6\,^{\circ}$C at low wind speeds but decreases to $0.2\,^{\circ}$C for high winds (e.g., Campbell, 1969; Burns and Sun, 2000). It is also well-known that T_s^{air} can contain a significant bias relative to true T due to uncertainties in the sonic path length (Loescher et al., 2005). Therefore, we adjust T_s^{air} with a linear fit to T_{asp} (the coefficients of the fit are listed in Fig. 5).

From Fig. 5 it can be seen that, during both day and night and for ver3 and ver4 CSATs, T_s^{air} shows a systematic decrease on the order of $0.2\,^{\circ}$C as U increases from around 8 to 15 m s^{-1}. This negative T_s^{air} error correlated with increasing U explains the positive H_{CSAT} error in the NWT data. Since w' is negatively correlated with u' in the surface layer and the T_s' error is also negatively correlated with u', the $\overline{w'T_s'}$ error is positive, as observed.

3.2 Consideration of the surface energy balance

As mentioned in the introduction, Turnipseed et al. (2002) found that the nocturnal SEB closure during high winds varied between 0.2–0.6. In Fig. 6, the SEB is calculated using H_{CSAT} (CU ver3) and $H_{T_{tc}}$ (1-Hz). As one would expect, the SEB with H_{CSAT} (CU ver3) closely matches the results of Turnipseed et al. (2002). At night (Fig. 6b), the SEB peaks at ≈0.7 for moderate U, and then becomes negative as U increases (or as friction velocity u_* increases as shown in Fig. 7 of Turnipseed et al., 2002). Also similar to Turnipseed et al. (2002), we find the nocturnal SEB with R_{net} from the Q*7.1 sensor is about 15 % closer to closing the SEB than with the CNR-1 sensor. For low winds, drainage flows form at the NWT site (Yi et al., 2005; Burns et al., 2011) and result in

near-zero nocturnal SEB values due to decoupling, strong horizontal advection of temperature, and practical difficulties with the flux calculation (e.g., Mahrt, 2010). These low-wind conditions require knowledge of horizontal advection for a more complete understanding (Sun et al., 2007; Yi et al., 2008).

5   During the day (Fig. 6a), the SEB using $H_{T_{tc}}$ and H_{CSAT} diverge at $U \approx 6\,\mathrm{m\,s^{-1}}$. For $U > 13\,\mathrm{m\,s^{-1}}$, the SEB with H_{CSAT} is close to 1. Knowing about the H_{CSAT} error in high winds (e.g., as discussed in Sect. 3.1 and shown in Fig. 3a) suggests that the daytime SEB approaching 1 is an artifact. In contrast, with $H_{T_{tc}}$, both the daytime and nighttime SEB values for $U > 6\,\mathrm{m\,s^{-1}}$ are in reasonable agreement at SEB ≈ 0.65–0.75, and there

10 is almost no dependence of the SEB on U. Unless there is a physical reason for the SEB to change with higher wind speeds, using $H_{T_{tc}}$ appears more reasonable than H_{CSAT}. If true, SEB closure at NWT without considering the storage terms is around 70 %. Taking into account the storage terms in Eq. (4) and the slight underestimation of $H_{T_{tc}}$ (1-Hz) we would expect the SEB closure to improve by about 10–15 %.

15 To better estimate the magnitude (in $\mathrm{W\,m^{-2}}$) of the SEB deficit we consider the 2006–2008 mean nocturnal values of R_{net} from the CNR-1 ($\approx -85\,\mathrm{W\,m^{-2}}$) and Q*7.1 ($\approx -60\,\mathrm{W\,m^{-2}}$) sensors. This difference of $25\,\mathrm{W\,m^{-2}}$ results in a 15 % difference in the SEB (Fig. 6b). These two R_{net} sensors are known to be accurate to only $20\,\mathrm{W\,m^{-2}}$ (Brotzge and Duchon, 2000; Foken, 2008; Michel et al., 2008) and within complex ter-

20 rain radiation measurements are complicated (Oliphant et al., 2003). This suggests that a "field-calibration" of the current radiation sensors to a high-accuracy radiometer (e.g., Burns et al., 2003) could improve our understanding of the surface energy budget at the site, and possibly, help explain the remaining lack of closure. Other factors that might cause the lack of closure are discussed elsewhere (e.g., Turnipseed et al., 2002;

25 Foken, 2008; Foken et al., 2011).

4   Conclusions

We compared H calculated using sonic anemometer temperature to H calculated with a co-located thermocouple and found U-dependent H differences on the order of $250\,\mathrm{W\,m^{-2}}$ at high wind speeds. To better understand these H differences, we considered the sur-

5   face energy budget. Using $H_{T_{tc}}$, the daytime and nighttime SEB values for $U > 6\,\mathrm{m\,s^{-1}}$ were fairly consistent (between 0.65–0.75). In contrast, using H_{CSAT} the SEB values in strong winds vary from below 0 (at night) to around 1 (during the day). Because there is no physical explanation for the wide variation in SEB with H_{CSAT}, we conclude that H calculated with the thermocouple is more reasonable. From analysis of the spectra and

10   co-spectra of $\overline{w'T'}$ in high winds, we conclude there is spurious correlation between w' and T_s' that lead to positive increases in H_{CSAT}. At night H is typically negative, and, for strong winds, the $\overline{w'T_s'}$ correlation error makes the magnitude of nocturnal H_{CSAT} smaller than it should be. Because T_{tc} and T_s are both correlated with w' from the same CSAT, we conclude that T_s is the primary source of the error.

15   We have been in contact with Campbell Scientific, Inc. regarding our observed heat flux discrepancies. They subsequently performed their own independent experiments to confirm the sonic temperature issues we have presented. Their preliminary results with a CSAT ver4 indicate that the issue occurs at all wind speeds, but is significant for $U > 8\,\mathrm{m\,s^{-1}}$. Campbell Scientific, Inc. is currently working to better quantify the

20   magnitude of the error and will mitigate it with future hardware and/or software changes.
Though our study examines one specific model of sonic anemometer, the tests we have outlined with a thermocouple could (and should) be used with any field-deployed sonic anemometer. Furthermore, in a broader context, our temperature comparison shows the added value of *independent*, co-located, in-situ measurements in environ-

25   mental research. Previous comparisons of sonic anemometers by Loescher et al. (2005) were very thorough, but performed the comparison up to a wind speed of $\approx 6\,\mathrm{m\,s^{-1}}$ so any issues at higher wind speeds were undetected. This emphasizes an important advantage of long-term in-situ comparisons – they cover the range of the

observation. In short, our study provides a practical example of how valuable in-situ comparisons can be in evaluating sensor performance.

References

10 Blanken, P. D., Black, T. A., Yang, P. C., Neumann, H. H., Nesic, Z., Staebler, R., den Hartog, G., Novak, M. D., and Lee, X.: Energy balance and canopy conductance of a boreal aspen forest: Partitioning overstory and understory components, J. Geophys. Res.-Atmos., 102, 28915–28927, 1997. 448

Blanken, P. D., Black, T. A., Neumann, H. H., Den Hartog, G., Yang, P. C., Nesic, Z., Staebler,
15 R., Chen, W., and Novak, M. D.: Turbulent flux measurements above and below the overstory of a boreal aspen forest, Bound.-Lay. Meteorol., 89, 109–140, 1998. 454

Brotzge, J. A. and Duchon, C. E.: A Field Comparison among a Domeless Net Radiometer, Two Four-Component Net Radiometers, and a Domed Net Radiometer, J. Atmos. Ocean. Tech., 17, 1569–1582, doi:10.1175/1520-0426(2000)017<1569:AFCAAD>2.0.CO;2, 2000.
20 457

Burns, S. P. and Sun, J.: Thermocouple temperature measurements from the CASES-99 main tower, in: 14th Symposium on Boundary Layer and Turbulence, Amer. Meteor. Soc., Snow-mass, Colorado, 358–361, 2000. 456

Burns, S. P., Sun, J., Delany, A. C., Semmer, S. R., Oncley, S. P., and Horst, T. W.: A field
25 intercomparison technique to improve the relative accuracy of longwave radiation measure-ments and an evaluation of CASES-99 pyrgeometer data quality, J. Atmos. Ocean. Tech., 20, 348–361, doi:10.1175/1520-0426(2003)020<0348:AFITTI>2.0.CO;2, 2003. 457

Burns, S. P., Sun, J., Lenschow, D. H., Oncley, S. P., Stephens, B. B., Chuixiang, Y., Anderson, D. E., Hu, J., and Monson, R. K.: Atmospheric stability effects on wind fields and scalar mixing within and just above a subalpine forest in sloping terrain, Bound.-Lay. Meteorol., 138, 231–262, doi:10.1007/s10546-010-9560-6, 2011. 456

5 Campbell, G. S.: Measurement of air temperature fluctuations with thermocouples, Tech. Rep. ECOM-5273, Atmospheric Sciences Laboratory, White Sands Missile Range, 10 pp., 1969. 456

Campbell Scientific: CSAT3 Three Dimensional Sonic Anemometer Manual (Revision 10/11), available at: www.campbellsci.com, last access: 10 January 2012, Campbell Scientific, Inc.,
10 Logan, Utah, 70 pp., 2011. 451, 452

Foken, T.: The energy balance closure problem: An overview, Ecol. Appl., 18, 1351–1367, 2008. 448, 449, 457

Foken, T., Aubinet, M., Finnigan, J. J., Leclerc, M. Y., Mauder, M., and Paw U, K. T.: Results of a panel discussion about the energy balance closure correction for trace gases, B. Am.
15 Meteorol. Soc., 92, ES13–ES18, 2011. 449, 457

Franssen, H. J. H., Stöckli, R., Lehner, I., Rotenberg, E., and Seneviratne, S. I.: Energy balance closure of eddy-covariance data: A multisite analysis for European FLUXNET stations, Agr. Forest Meteorol., 150, 1553–1567, doi:10.1016/j.agrformet.2010.08.005, 2010. 449

Friehe, C. A., Shaw, W. J., Rogers, D. P., Davidson, K. L., Large, W. G., Stage, S. A., Crescenti,
20 G. H., Khalsa, S. J. S., Greenhut, G. K., and Li, F.: Air-sea fluxes and surface-layer turbulence around a sea-surface temperature front, J. Geophys. Res., 96, 8593–8609, 1991. 455

Garratt, J. R.: The atmospheric boundary layer, Cambridge University Press, Cambridge, 316 pp., 1992. 448

Horst, T. W. and Lenschow, D. H.: Attenuation of Scalar Fluxes Measured with Spatially-
25 displaced Sensors, Bound.-Lay. Meteorol., 130, 275–300, 2009. 454

Kaimal, J. C. and Businger, J. A.: A continuous wave sonic anemometer-thermometer, J. Appl. Meteorol., 2, 156–164, 1963. 450

Kaimal, J. C. and Finnigan, J. J.: Atmospheric boundary layer flows: their structure and measurement, Oxford University Press, New York, 289 pp., 1994. 454

30 Kaimal, J. C. and Gaynor, J. E.: Another look at sonic thermometry, Bound.-Lay. Meteorol., 56, 401–410, 1991. 450

Title Page

Abstract | Introduction

Conclusions | References

Tables | Figures

|◄ | ►|

◄ | ►

Back | Close

Full Screen / Esc

Printer-friendly Version

Interactive Discussion

Lanzinger, E. and Langmack, H.: Measuring Air Temperature by using an Ultrasonic Anemometer, in: Technical Conference on Meteorological and Environmental Instruments and Methods of Observation (TECO-2005), WMO Tech. Doc. No. 1265; IOM Report No. 82, http://www.wmo.int/pages/prog/www/IMOP/publications/IOM-82-TECO_2005/Programme_index.html last access: 10 January 2012, World Meteorological Organization, Geneva, Switzerland, p.P3(9), 2005. 453

Loescher, H. W., Ocheltree, T., Tanner, B., Swiatek, E., Dano, B., Wong, J., Zimmerman, G., Campbell, J., Stock, C., Jacobsen, L., Shiga, Y., Kollas, J., Liburdy, J., and Law, B. E.: Comparison of temperature and wind statistics in contrasting environments among different sonic anemometer-thermometers, Agr. Forest Meteorol., 133, 119–139, 2005. 450, 451, 456, 458

Mahrt, L.: Computing turbulent fluxes near the surface: needed improvements, Agr. Forest Meteorol., 150, 501–509, 2010. 457

Massman, W. and Clement, R.: Uncertainty in Eddy Covariance Flux Estimates Resulting from Spectral Attenuation, in: Handbook of Micrometeorology, edited by: Lee, X., Massman, W., and Law, B., vol. 29 of Atmospheric and Oceanographic Sciences Library, Springer, The Netherlands, 67–99, 2005. 454

Michel, D., Philipona, R., Ruckstuhl, C., Vogt, R., and Vuilleumier, L.: Performance and uncertainty of CNR1 net radiometers during a one-year field comparison, J. Atmos. Ocean. Technol., 25, 442–451, 2008. 457

Monson, R. K., Turnipseed, A. A., Sparks, J. P., Harley, P. C., Scott-Denton, L. E., Sparks, K., and Huxman, T. E.: Carbon sequestration in a high-elevation, subalpine forest, Global Change Biol., 8, 459–478, 2002. 450

Oliphant, A. J., Spronken-Smith, R. A., Sturman, A. P., and Owens, I. F.: Spatial variability of surface radiation fluxes in mountainous terrain, J. Appl. Meteorol., 42, 113–128, 2003. 457

Oncley, S. P., Foken, T., Vogt, R., Kohsiek, W., DeBruin, H. A. R., Bernhofer, C., Christen, A., van Gorsel, E., Grantz, D., Feigenwinter, C., Lehner, I., Liebethal, C., Liu, H., Mauder, M., Pitacco, A., Ribeiro, L., and Weidinger, T.: The Energy Balance Experiment EBEX-2000, Part I: Overview and energy balance, Bound.-Lay. Meteorol., 123, 1–28, 2007. 448, 452

Patton, E. G., Horst, T. W., Sullivan, P. P., Lenschow, D. H., Oncley, S. P., Brown, W. O. J., Burns, S. P., Guenther, A. B., Held, A., Karl, T., Mayor, S. D., Rizzo, L. V., Spuler, S. M., Sun, J., Turnipseed, A. A., Allwine, E. J., Edburg, S. L., Lamb, B. K., Avissar, R., Calhoun, R. J., Kleissl, J., Massman, W. J., Paw, K. T., and Weil, J. C.: The Canopy Horizontal Array

Turbulence Study, B. Am. Meteorol. Soc., 92, 593–611, 2011. 455

Schotanus, P., Nieuwstadt, F. T. M., and De Bruin, H. A. R.: Temperature-measurement with a sonic anemometer and its application to heat and moisture fluxes, Bound.-Lay. Meteorol., 26, 81–93, 1983. 450, 451

5 Stewart, J. B. and Thom, A. S.: Energy budgets in pine forest, Q. J. Roy. Meteorol. Soc., 99, 154–170, 1973. 448

Sun, J., Burns, S. P., Delany, A. C., Oncley, S. P., Turnipseed, A. A., Stephens, B. B., Lenschow, D. H., LeMone, M. A., Monson, R. K., and Anderson, D. E.: CO_2 transport over complex terrain, Agr. Forest Meteorol., 145, 1–21, doi:10.1016/j.agrformet.2007.02.007, 2007. 457

10 Timouk, F., Kergoat, L., Mougin, E., Lloyd, C. R., Ceschia, E., Cohard, J. M., de Rosnay, P., Hiernaux, P., Demarez, V., and Taylor, C. M.: Response of surface energy balance to water regime and vegetation development in a Sahelian landscape, J. Hydrol., 375, 178–189, 2009. 449

Turnipseed, A. A., Blanken, P. D., Anderson, D. E., and Monson, R. K.: Energy budget above a
15 high-elevation subalpine forest in complex topography, Agr. Forest Meteorol., 110, 177–201, 2002. 449, 450, 452, 455, 456, 457, 469

Turnipseed, A. A., Anderson, D. E., Blanken, P. D., Baugh, W. M., and Monson, R. K.: Airflows and turbulent flux measurements in mountainous terrain. Part 1: canopy and local effects, Agr. Forest Meteorol., 119, 1–21, 2003. 450

20 Wilczak, J. M., Oncley, S. P., and Stage, S. A.: Sonic anemometer tilt correction algorithms, Bound.-Lay. Meteorol, 99, 127–150, 2001. 452

Wilson, K., Goldstein, A., Falge, E., Aubinet, M., Baldocchi, D., Berbigier, P., Bernhofer, C., Ceulemans, R., Dolman, H., Field, C., Grelle, A., Ibrom, A., Law, B. E., Kowalski, A., Meyers, T., Moncrieff, J., Monson, R., Oechel, W., Tenhunen, J., Valentini, R., and Verma, S.: Energy
25 balance closure at FLUXNET sites, Agr. Forest Meteorol., 113, 223–243, 2002. 449

Yi, C., Monson, R. K., Zhai, Z. Q., Anderson, D. E., Lamb, B., Allwine, G., Turnipseed, A. A., and Burns, S. P.: Modeling and measuring the nocturnal drainage flow in a high-elevation, subalpine forest with complex terrain, J. Geophys. Res., 110, D22303, doi:10.1029/2005JD006282, 2005. 456

30 Yi, C., Anderson, D. E., Turnipseed, A. A., Burns, S. P., Sparks, J. P., Stannard, D. I., and Monson, R. K.: The contribution of advective fluxes to net ecosystem exchange in a high-elevation, subalpine forest, Ecol. Appl., 18, 1379–1390, doi:10.1890/06-0908.1, 2008. 457

Sensible heat flux in high winds

S. P. Burns et al.

Table 1. A summary of NWT AmeriFlux tower temperature measurements used in our study.

Sensor	Acronym	Sensor Height (cm)	Horizontal Separation[a] (cm)	Sample Rate[b]	Deployment Dates	Additional Comments
Vaisala HMP35-D	T_{asp}	2150	≈90	1	1 Nov 1998–present	slow-response platinum resistance thermometer in a mechanically-aspirated housing
E-type Thermocouple	T_{tc} (1-Hz)	2198	≈136	1	20 Aug 2002–present	wire dia = 0.254 mm, unaspirated
	T_{tc} (10-Hz)	2148	<5	10	5 May 2010–present	wire dia = 0.254 mm, unaspirated
Campbell Scientific CSAT3 Three Dimensional Sonic Ane-mometer[d]	CU CSAT[c], ver3	2150	0	10	1 Nov 1998–14 Jan 2008	sn 0226, embedded code version 3
	CU CSAT[c], ver3	2150	0	10	14 Jan 2008–21 Feb 2008	sn 0536, embedded code version 3 (on loan from EOL)
	CU CSAT[c], ver3	2150	0	10	21 Feb 2008–31 Oct 2008	sn 0438, embedded code version 3
	CU CSAT[c], ver4	2150	0	10	31 Oct 2008–28 Sep 2010	sn 0328, embedded code version 4, recalibrated in Oct 2008
	CU CSAT[c], ver4	2150	0	10	28 Sep 2010–present	sn 0198, embedded code version 4
	EOL CSAT, ver3	2150	≈160	10	27 Sep 2009–17 Jan 2010	sn 0674, embedded code version 3
	EOL CSAT, ver4	2150	≈160	10	17 Jan 2010–21 Oct 2011	on 17 Jan 2010, changed sn 0674 control box from embedded code version 3 to version 4
	EOL CSAT, ver3	2150	≈160	10	21 Oct 2011–present	on 21 Oct 2011, changed sn 0674 control box back to version 3

[a] Horizontal distance from the University of Colorado (CU) CSAT sensor.

[b] Number of samples per second (Hz).

[c] The 2150 cm CU CSAT is used to determine the horizontal wind speed (U).

[d] The CSAT3 sonic temperature (T_s) corrected for humidity is $T_s^{air} = T_s (1 + 0.51q)^{-1}$ where q is specific humidity. Also, CSAT data deemed unacceptable by the CSAT diagnostic flag were replaced with a linear fit between valid samples (for low wind wind speeds data were rarely flagged, but for higher winds around 2–4 % of the samples were flagged).

S. P. Burns et al.
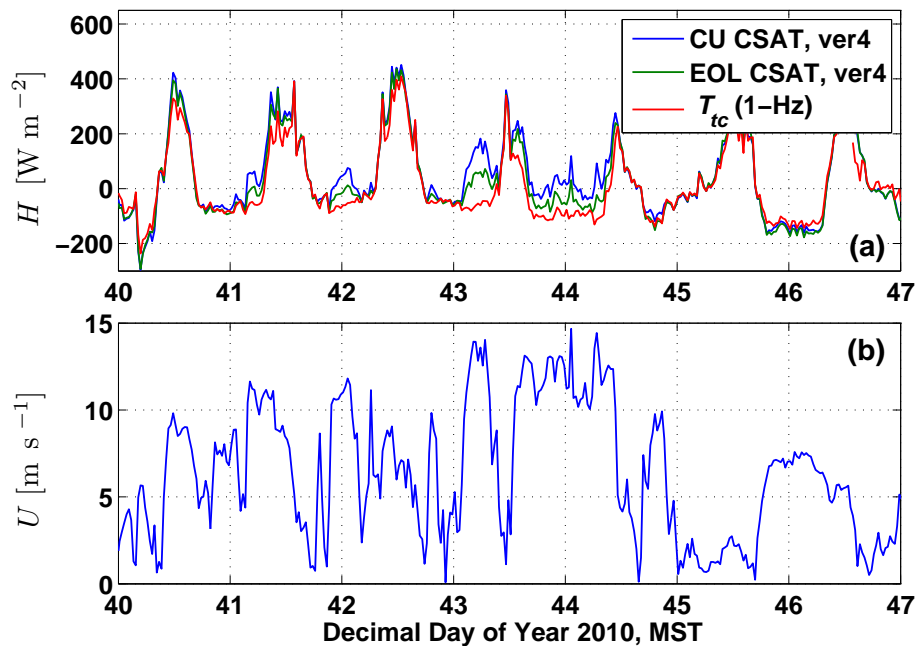
Fig. 1. Time series of 21.5 m **(a)** sensible heat flux H and **(b)** horizontal wind speed U. H is calculated using different temperature sensors as specified in the legend (see Table 1 for details).
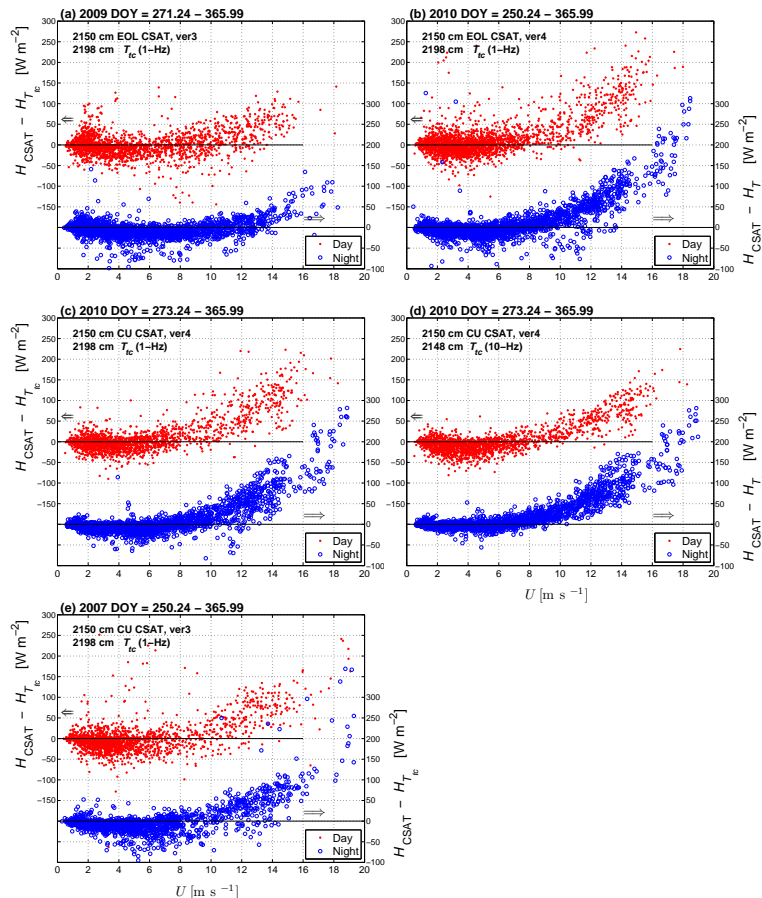
Fig. 2. The sensible heat flux difference calculated with the CSAT and thermocouple ($H_{CSAT} - H_{T_{tc}}$) versus the 21.5 m horizontal wind speed U. In **(a)**–**(e)**, the time period (day of year, DOY) is specified along with the particular CSAT and thermocouple used (upper-left corner). (See Table 1 for sensor details.) Each point represents H calculated over 30 min, then separated into daytime (left-side axis) and nighttime (right-side axis) periods as shown by the horizontal arrows and legend.

Fig. 3. Mean **(a)** daytime and **(b)** nighttime values of: vertical wind spectra S_w, temperature (either T_s or T_{tc}, see legend and Table 1) spectra S_T, $\overline{w'T'}$ cospectra $(Co)_{wT}$, and sensible heat flux H ogive versus frequency f. These are 30-min periods from November, 2010 selected for wind speed U greater than $10\,\text{m s}^{-1}$ (the number of 30-minute periods that match our criteria is listed above the S_T panel). The dashed line shows a $-2/3$ slope. Note that the S_w lines from the two CSATs are nearly indistinguishable from each other.

Fig. 4. The (left column) $\overline{w'T'}$ cospectra $(Co)_{wT}$ and (right column) temperature spectra S_T for medium- and low-wind conditions (see Fig. 3 for the legend and further details).
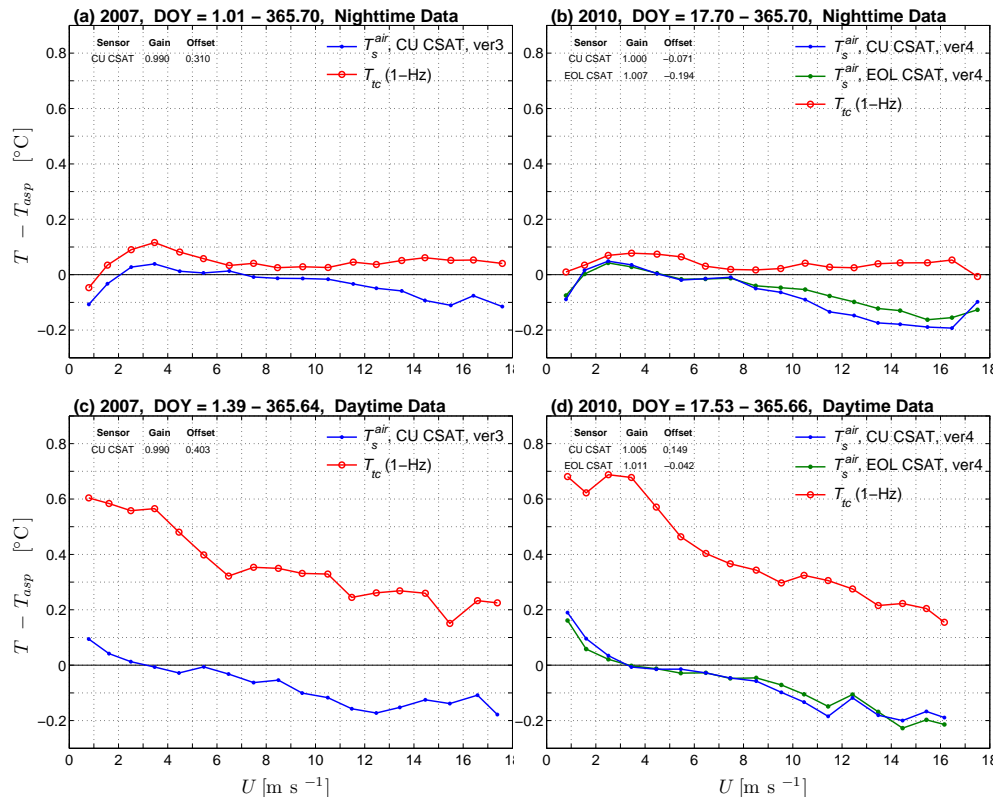
Fig. 5. The **(a, b)** nighttime and **(c, d)** daytime mean temperature difference ($T - T_{\mathrm{asp}}$) versus 21.5 m horizontal wind speed U. T_{asp} is measured within a mechanically-aspirated housing and T is from either the humidity-corrected CSATs (T_s^{air}) or a thermocouple (T_{tc}, 1-Hz) as specified in the legend (also see Table 1). T_s^{air} has been linearly adjusted to T_{asp} using the gain and offset shown in the upper left corner of each panel. The time period (day of year, DOY) used for each panel is shown.
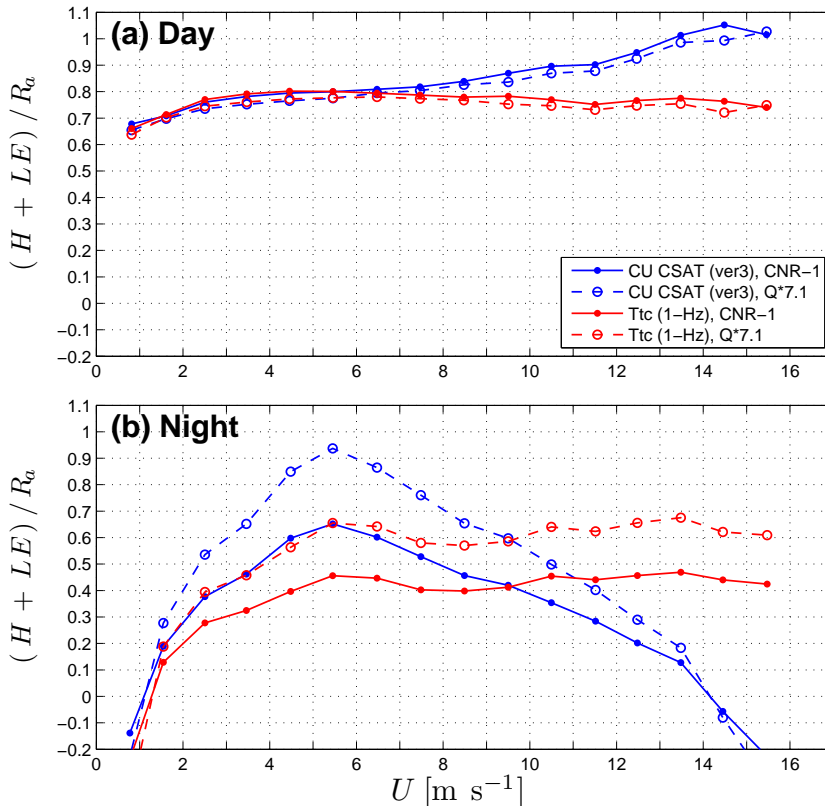
Fig. 6. The surface energy balance [SEB = $(H + LE)/R_a$] versus horizontal wind speed U from years 2006–2008 for **(a)** daytime and **(b)** nighttime conditions ($R_a = R_{net} - G$ is the available energy, see text for details). The sensors used to calculate H (CU CSAT, ver3 or T_{tc}, 1-Hz) and R_{net} (Kipp and Zonen, model CNR-1 or REBS, model Q*7.1) are specified in the legend. (This figure is comparable to Fig. 7 in Turnipseed et al., 2002.)